

# FDTD Characterization of Waveguide-Probe Structures

Emmanouil Tentzeris, *Member, IEEE*, Michael Krumpholz, *Member, IEEE*, Nihad Dib, Jong-Gwan Yook, and Linda P. B. Katehi, *Fellow, IEEE*

**Abstract**—The finite-difference time-domain (FDTD) technique is applied in the calculation of the  $S$ -parameters of diode mounting and waveguide-probe structures. The influence of the critical geometrical design parameters on the coupling of the coplanar feedline probe to the waveguide is investigated. A waveguide absorber based on analytic Green's functions is used to minimize the reflections over a wide band of frequencies.

**Index Terms**—Diakoptics, finite-difference time-domain, Green's functions, waveguide absorber, waveguide probes.

## I. INTRODUCTION

**S**IGNIFICANT attention is being devoted these days to the analysis and design of waveguide probes [1]–[4]. Many different configurations of waveguide probes are used either to sense the modal propagation inside the waveguides or to mount active elements inside cavities. The common design objective is to maximize the coupling between the probe and waveguide over the widest possible frequency range. The characterization of waveguide probes demands an accurate calculation of the scattering parameters over a wide band of frequencies. In this paper, the finite-difference time-domain (FDTD) method [5] is used in the RF characterization of diode mounting and waveguide-probe structures. The waveguide-probe geometry analyzed in this paper is shown in Fig. 1. The probe is fed by a shielded coplanar line and has the shape of a patch. It is inserted into the waveguide through a slot and is supported by a dielectric substrate, which is not connected to any waveguide wall. The dimensions of the probe as well as the thickness and dielectric constant of the substrate are of critical importance to achieve broad-band coupling and low reflection loss.

Manuscript received April 8, 1996; revised March 2, 1998. This work was supported by the NATO Science Committee under a scholarship through the German Academic Exchange Service, and by the U.S. Army Research Office.

E. Tentzeris was with the Radiation Laboratory, Department of Electrical Engineering and Computer Science, University of Michigan, Ann Arbor, MI 48109-2122 USA. He is now with the School of Electrical and Computer Engineering, Georgia Institute of Technology, Atlanta, GA 30332-0250 USA (e-mail: etentze@ece.gatech.edu).

M. Krumpholz was with the Radiation Laboratory, Department of Electrical Engineering and Computer Science, University of Michigan, Ann Arbor, MI 48109-2122, USA. He is now with the Daimler-Benz Corporation, Stuttgart, Germany.

N. Dib is with the Electrical Engineering Department, Jordan University of Science and Technology, Irbid 22110, Jordan.

J.-G. Yook and L. P. B. Katehi are with the Radiation Laboratory, Department of Electrical Engineering and Computer Science, University of Michigan, Ann Arbor, MI 48109-2122 USA.

Publisher Item Identifier S 0018-9480(98)07242-1.

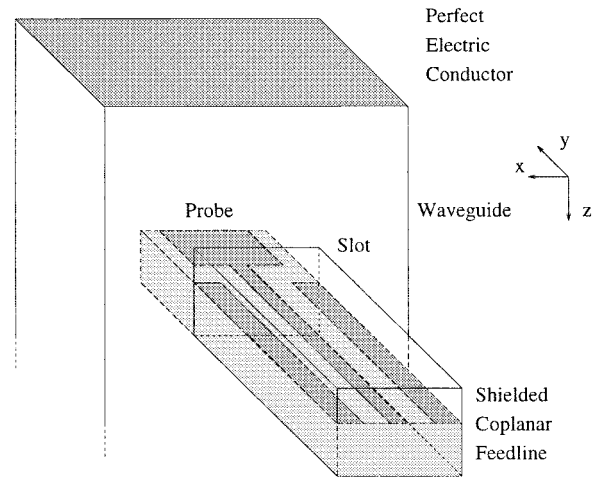


Fig. 1. Waveguide-probe structure.

Usually more than one mode is excited inside the rectangular waveguide, making the numerical simulation tedious when using the conventional absorbing boundary conditions (ABC's) [6], [7]. These ABC's specify the tangential electric-field components at the boundary of the mesh in such a way that waves are not reflected. For TEM structures, the waves will be normally incident to the boundaries of the mesh, thus requiring a simple approximate ABC—Mur's first-order ABC [6]. The assumption of normal incidence is not valid for the fringing fields propagating tangential to the walls. For this reason, for non-TEM structures, the superabsorption boundary condition [7] is used in conjunction with Mur's absorber for better accuracy. This combination results in an improvement with respect to the reflection coefficient. However, despite the use of a superabsorber, when the frequency range of interest becomes large, significant reflections occur, even if there is only one propagating mode. To overcome this difficulty, numerous approaches have been proposed. The technique of diakoptics [8], initially developed for transmission-line matrix (TLM) [9] and, later, for FDTD [10], used in conjunction with the modal Green's function has been successfully applied to TLM [11]–[13]. In the analogous FDTD approach [14], the fields are decomposed into incident and reflected wave amplitudes ("TLM" approach) and the characteristic impedance is used for the calculation of the reflected wave amplitudes. A similar absorber based on a circuit (voltage-current) approach has been proposed by Moglie *et al.* [15]. Due to the field decomposition, both of these approaches are characterized

by higher memory and execution time requirements than the conventional FDTD absorbers.

In contrast to these approaches, we derive the diakoptics technique directly from Maxwell's equations following an approach similar to [16], and we use only total field values. The absorber proposed in this paper is based on the analytic Green's functions of the waveguide modes. These Green's functions are used to calculate the tangential electric (for TE modes) and magnetic (for TM modes) field components located at the boundary of the mesh. The tangential fields one cell away from the boundary are decomposed into modes and, for each mode, the tangential field at the boundary is calculated by taking the convolution of the mode amplitude and Green's function for this mode with respect to time. For simplicity, we consider only TE propagating modes, while the approach for the TM propagating modes is dual and straightforward. A similar approach based on numerical Green's functions has been presented in [17]. This approach requires the numerical evaluation of each mode's Green's function that is obtained by running an FDTD simulation for each mode and/or the application of the FD<sup>2</sup> principles. On the contrary, the absorber proposed in this paper analytically evaluates the Green's functions by applying the inverse Fourier transform to the well-known expressions in the frequency domain. Thus, similar accuracy is obtained without a significant computational overhead.

The Gabor function is used as an excitation for the waveguide mounting structures. A parametric study of the scattering parameters of the waveguide-probe geometry, shown in Fig. 1, is performed for a number of geometrical parameters, and the results are verified by data obtained from the finite-element method (FEM) and measurements.

## II. OVERVIEW OF THE FDTD TECHNIQUE

Yee's FDTD scheme [5] discretizes Maxwell's curl equations by approximating the time and space first-order partial derivatives with centered differences. For the  $H$ -field, it is given by

$$\begin{aligned} & l+1/2 H_{i,j+1/2,k+1/2}^x - l-1/2 H_{i,j+1/2,k+1/2}^x \\ &= \frac{\Delta t}{\mu_0} \left( \frac{l E_{i,j+1/2,k+1/2}^y - l E_{i,j+1/2,k}^y}{\Delta z} \right. \\ & \quad \left. - \frac{l E_{i,j+1,k+1/2}^z - l E_{i,j,k+1/2}^z}{\Delta y} \right) \end{aligned} \quad (1)$$

$$\begin{aligned} & l+1/2 H_{i+1/2,j,k+1/2}^y - l-1/2 H_{i+1/2,j,k+1/2}^y \\ &= \frac{\Delta t}{\mu_0} \left( \frac{l E_{i+1,j,k+1/2}^z - l E_{i,j,k+1/2}^z}{\Delta x} \right. \\ & \quad \left. - \frac{l E_{i+1/2,j,k+1}^x - l E_{i+1/2,j,k}^x}{\Delta z} \right) \end{aligned} \quad (2)$$

$$\begin{aligned} & l+1/2 H_{i+1/2,j+1/2,k}^z - l-1/2 H_{i+1/2,j+1/2,k}^z \\ &= \frac{\Delta t}{\mu_0} \left( \frac{l E_{i+1/2,j+1,k}^x - l E_{i+1/2,j,k}^x}{\Delta y} \right. \\ & \quad \left. - \frac{l E_{i+1,j+1/2,k}^y - l E_{i,j+1/2,k}^y}{\Delta x} \right). \end{aligned} \quad (3)$$

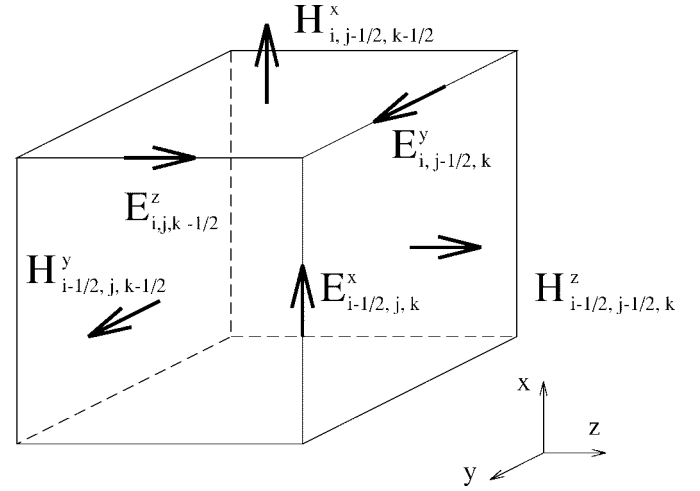


Fig. 2. Yee's FDTD cell.

The equations for the  $E$ -field are dual to the above. The six field components are considered to be interleaved in space, as shown in Fig. 2. The indexes  $i$ ,  $j$ ,  $k$ , and  $l$  are related to the space and time coordinates via  $x = i\Delta x$ ,  $y = j\Delta y$ ,  $z = k\Delta z$ , and  $t = l\Delta t$ , where  $\Delta x$ ,  $\Delta y$ ,  $\Delta z$ , and  $\Delta t$  represent the unit space interval in the  $x$ -,  $y$ -,  $z$ -direction, and unit time interval, respectively. The electric conductors are assumed to be perfectly conducting with zero thickness and, as an excitation, we chose the Gabor function given by

$$f(t) = e^{-((t-t_0)/(pw))^2} \sin(ut) \quad (4)$$

where  $pw = 2 \cdot (\sqrt{6}/\pi)(f_{\max} - f_{\min})$ ,  $t_0 = 2pw$ ,  $w = \pi(f_{\min} + f_{\max})$ . By modifying the parameters  $pw$  and  $w$ , we can practically restrict the frequency spectrum of the Gabor function to the interval  $[f_{\min}, f_{\max}]$ . As a result, the envelope of the Gabor function represents a Gaussian function in both time and frequency domain.

## III. ABSORBER DESCRIPTION

For the sake of simplicity in presentation, we consider only TE <sub>$m,n$</sub>  modes, propagating in the  $z$ -direction, and assume that the waveguide cross section is located on the  $xy$ -plane. For the tangential magnetic field adjacent to the boundary of the mesh at  $k = n_z - 0.5$ , (1) and (2) are simplified to

$$\begin{aligned} & l+1/2 H_{i,j+1/2,n_z-0.5}^x - l-1/2 H_{i,j+1/2,n_z-0.5}^x \\ &= \frac{\Delta t}{\mu_0} \left( \frac{l E_{i,j+1/2,n_z}^y - l E_{i,j+1/2,n_z-1}^y}{\Delta z} \right) \end{aligned} \quad (5)$$

$$\begin{aligned} & l+1/2 H_{i+1/2,j,n_z-0.5}^y - l-1/2 H_{i+1/2,j,n_z-0.5}^y \\ &= \frac{\Delta t}{\mu_0} \left( \frac{l E_{i+1/2,j,n_z-1}^x - l E_{i+1/2,j,n_z}^x}{\Delta z} \right). \end{aligned} \quad (6)$$

The absorber is used to calculate the tangential electric-field components at the boundary of the mesh ( $k = n_z$ ) from the tangential electric-field components one cell away from the boundary plane ( $k = n_z - 1$ ). The tangential magnetic-field components  $H_{i,j,n_z-0.5}^x$  and  $H_{i,j,n_z-0.5}^y$  are updated using (5) and (6), and depend both on the values of the electric-field components calculated by Yee's FDTD scheme and on

the values of the electric-field components calculated by the absorber. Using (3), the normal magnetic-field components at  $k = n_z$ ,  $H_{i+1/2, j+1/2, n_z}^z$  may be calculated from  $E_{i+1/2, j, n_z}^x$  and  $E_{i, j+1/2, n_z}^y$ . Thus, for the  $\text{TE}_{m,n}^z$  modes, the normal magnetic-field components are also determined so that the reflection from the boundary is minimized. A similar argument can be used for the position of the absorber for the  $\text{TM}_{m,n}^z$  modes.

In order to derive the absorber based on the analytic Green's functions, we start with the wave equation in Cartesian coordinates

$$\nabla^2 F - \frac{1}{c^2} \frac{\partial^2 F}{\partial t^2} = \left( \frac{\partial^2}{\partial x^2} + \frac{\partial^2}{\partial y^2} + \frac{\partial^2}{\partial z^2} - \frac{1}{c^2} \frac{\partial^2}{\partial t^2} \right) F = 0 \quad (7)$$

where  $F$  indicates the tangential electric-field components  $E^x(x, y, z, t)$ ,  $E^y(x, y, z, t)$ , and  $c$  represents the velocity of light. The tangential electric-field components in the waveguide can be written as

$$E^x(x, y, z, t) = \sum_{m=0}^{\infty} \sum_{n=1}^{\infty} E_{m,n}^x(z, t) \cos(\beta_{x,m}x) \sin(\beta_{y,n}y) \quad (8)$$

$$E^y(x, y, z, t) = \sum_{m=1}^{\infty} \sum_{n=0}^{\infty} E_{m,n}^y(z, t) \sin(\beta_{x,m}x) \cos(\beta_{y,n}y) \quad (9)$$

where

$$\beta_{x,m} = \frac{m\pi}{a} \quad \beta_{y,n} = \frac{n\pi}{b} \quad (10)$$

$m, n \in N$ ,  $a \times b$  are the waveguide cross-section area and  $E_{m,n}^x(z, t)$  and  $E_{m,n}^y(z, t)$  are the modal coefficients given by

$$E_{m,n}^x(z, t) = \frac{2(2 - \delta_{m,0})}{ab} \int_0^a \int_0^b E^x(x, y, z, t) \cdot \cos\left(\frac{m\pi}{a}x\right) \sin\left(\frac{n\pi}{b}y\right) dx dy \quad (11)$$

$$E_{m,n}^y(z, t) = \frac{2(2 - \delta_{n,0})}{ab} \int_0^a \int_0^b E^y(x, y, z, t) \cdot \sin\left(\frac{m\pi}{a}x\right) \cos\left(\frac{n\pi}{b}y\right) dx dy. \quad (12)$$

In (11) and (12),  $\delta_{m,0}$  is the Kronecker delta given by

$$\delta_{m,0} = \begin{cases} 1, & \text{for } m = 0 \\ 0, & \text{for } m \neq 0. \end{cases}$$

In view of the above, (7) yields

$$\frac{\partial^2 F_{m,n}(z, t)}{\partial z^2} - \left( \beta_{x,m}^2 + \beta_{y,n}^2 + \frac{1}{c^2} \frac{\partial^2}{\partial t^2} \right) F_{m,n}(z, t) = 0 \quad (13)$$

where  $F_{m,n}(z, t) = E_{m,n}^{x,y}(z, t)$ .

Applying the Fourier transformation ( $\bar{F}_{m,n}(z, \omega) = \mathcal{F}\{F_{m,n}(z, t)\}$ ) with the angular frequency  $\omega = 2\pi f$ , the

wave equation is transformed into the frequency domain, and (13) yields

$$\frac{\partial^2 \bar{F}_{m,n}(z, \omega)}{\partial z^2} - \left( \beta_{x,m}^2 + \beta_{y,n}^2 - \frac{\omega^2}{c^2} \right) \bar{F}_{m,n}(z, \omega) = 0. \quad (14)$$

Following a procedure analogous to [16] and assuming a given amplitude  $\bar{F}_{m,n}((n_z - 1)\Delta z, \omega)$  of the  $\text{TE}_{m,n}^z$  mode at  $k = n_z - 1$ , we obtain

$$\begin{aligned} \bar{F}_{m,n}(z, \omega) = & \frac{e^{j\beta_{z,mn}(z - (n_z - 1)\Delta z)}}{2} \\ & \cdot \left( \bar{F}_{m,n}((n_z - 1)\Delta z, \omega) \right. \\ & \quad \left. - \frac{j}{\beta_{z,mn}} \frac{\partial \bar{F}_{m,n}(z, \omega)}{\partial z} \Big|_{z=(n_z - 1)\Delta z} \right) \\ & + \frac{e^{-j\beta_{z,mn}(z - (n_z - 1)\Delta z)}}{2} \\ & \cdot \left( \bar{F}_{m,n}((n_z - 1)\Delta z, \omega) \right. \\ & \quad \left. + \frac{j}{\beta_{z,mn}} \frac{\partial \bar{F}_{m,n}(z, \omega)}{\partial z} \Big|_{z=(n_z - 1)\Delta z} \right) \end{aligned} \quad (15)$$

with

$$\beta_{z,mn} = \begin{cases} \frac{1}{c} \sqrt{\omega^2 - \omega_{c,mn}^2}, & \text{for } \omega \geq \omega_{c,mn} \\ -j \frac{1}{c} \sqrt{\omega_{c,mn}^2 - \omega^2}, & \text{for } \omega \leq \omega_{c,mn} \end{cases} \quad (16)$$

where  $\omega_{c,mn} = c\sqrt{(\beta_{x,m})^2 + (\beta_{y,n})^2}$  is the cutoff frequency of the  $\text{TE}_{m,n}^z$  mode. The function  $\bar{F}_{m,n}(z, \omega)$  has exponentially increasing and decreasing solutions with respect to  $z$  for  $\omega \leq \omega_{c,mn}$ . The exponentially increasing solutions have to vanish for  $z \rightarrow \infty$  for  $\omega \leq \omega_{c,mn}$ , thus, (15) yields

$$\bar{F}_{m,n}((n_z - 1)\Delta z, \omega) = \frac{j}{\beta_{z,mn}} \frac{\partial \bar{F}_{m,n}(z, \omega)}{\partial z} \Big|_{z=(n_z - 1)\Delta z} \quad (17)$$

and

$$\bar{F}_{m,n}(z, \omega) = \bar{G}_{\text{TE}_{m,n}^z}(z - (n_z - 1)\Delta z, \omega) \cdot \bar{F}_{m,n}((n_z - 1)\Delta z, \omega) \quad (18)$$

where  $\bar{G}_{\text{TE}_{m,n}^z}(z, \omega) = e^{-j\beta_{z,mn}z}$  is the Green's function for the  $\text{TE}_{m,n}^z$  modes. By satisfying (17),  $\bar{F}_{m,n}((n_z - 1)\Delta z, \omega)$  results in an outward propagating solution with respect to  $z$  for  $\omega \geq \omega_{c,mn}$  only. Thus, computation of  $\bar{F}_{m,n}(z, \omega)$  according to (18) requires no backward propagating solution.

Applying the convolution theorem [18], (18) in time domain reduces to

$$F_{m,n}(z, t) = \int_{-\infty}^{+\infty} G_{\text{TE}_{m,n}^z}(z - (n_z - 1)\Delta z, t - t') \cdot F_{m,n}((n_z - 1)\Delta z, t') dt' \quad (19)$$

where  $G_{\text{TE}_{m,n}^z}(z, t) = \mathcal{F}^{-1}\{\bar{G}_{\text{TE}_{m,n}^z}(z, \omega)\}$ . As a result, the tangential electric-field components at the boundary of the mesh at  $k = n_z$  are expressed in the following form:

$$F_{m,n}(n_z \Delta z, t) = \int_{-\infty}^{+\infty} G_{\text{TE}_{m,n}^z}(\Delta z, t - t') \cdot F_{m,n}((n_z - 1)\Delta z, t') dt'. \quad (20)$$

Following a procedure similar to [19],  $F_{m,n}((n_z - 1)\Delta z, t')$  can be expanded in a series of triangle basis functions in time-domain. Inserting this expansion in (20) and sampling  $F_{m,n}(n_z \Delta z, t)$  using delta functions with respect to time, we obtain

$$F_{m,n}(n_z \Delta z, l\Delta t) = \sum_{l'=-\infty}^{\infty} t_{-l'} G_{\text{TE}_{m,n}^z} \cdot F_{m,n}((n_z - 1)\Delta z, l'\Delta t) \quad (21)$$

where the discrete FDTD Green's function  $t_{-l'} G_{\text{TE}_{m,n}^z}$  may be calculated analytically by

$$\begin{aligned} t_{-l'} G_{\text{TE}_{m,n}^z} &= \int_{-\infty}^{+\infty} G_{\text{TE}_{m,n}^z}(\Delta z, l\Delta t - x) g(x) dx \\ &= \frac{1}{2\pi} \int_{-\infty}^{+\infty} \bar{G}_{\text{TE}_{m,n}^z}(\Delta z, \omega) \bar{g}(\omega) e^{j\omega l\Delta t} d\omega \end{aligned} \quad (22)$$

and  $x = t' - l'\Delta t$ . The triangle basis function is given by

$$g(x) = \begin{cases} 1 - \left| \frac{x}{\Delta t} \right|, & \text{for } |x| \leq \Delta t \\ 0, & \text{for } |x| \geq \Delta t. \end{cases}$$

and its Fourier transform is

$$\bar{g}(\omega) = \mathcal{F}\{g(t)\} = \Delta t \left[ \frac{\sin\left(\frac{\omega \Delta t}{2}\right)}{\frac{\omega \Delta t}{2}} \right]^2. \quad (23)$$

Due to causality, we have

$$t_{-l'} G_{\text{TE}_{m,n}^z} = 0 \quad \text{for } l < 0 \quad (24)$$

and, as a result,

$$F_{m,n}(n_z \Delta z, l\Delta t) = \sum_{l'=-\infty}^l t_{-l'} G_{\text{TE}_{m,n}^z} \cdot F_{m,n}((n_z - 1)\Delta z, l'\Delta t) \quad (25)$$

which represents the mathematical formulation of the Diakoptics technique.

As an example, let us consider the  $\text{TE}_{1,0}^z$  mode. For the  $y$ -component  $t_{-l'} E_{i,j,n_z}^y$  of the tangential electric field at  $k = n_z$ , (9) and (25) yield

$$t_{-l'} E_{i,j,n_z}^y = \sum_{l'=-\infty}^l t_{-l'} G_{\text{TE}_{1,0}^z} E_{1,0}^y((n_z - 1)\Delta z, l'\Delta t) \cdot \sin(\pi i \Delta x / a) \quad (26)$$

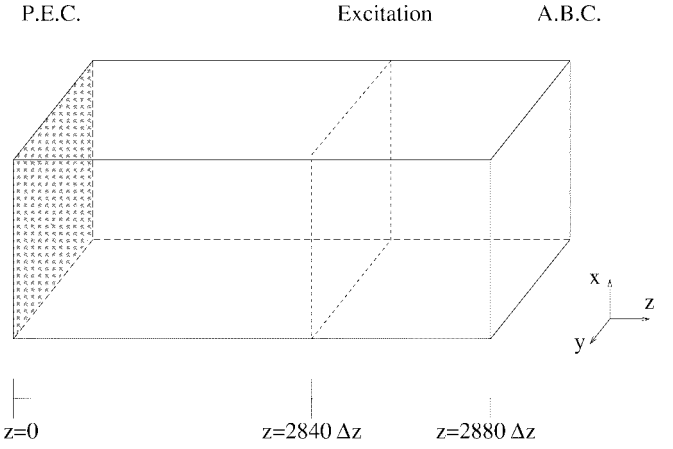


Fig. 3. Waveguide test structure.

where  $E_{1,0}^y((n_z - 1)\Delta z, l'\Delta t)$  may be calculated from (12). The discrete FDTD Green's function  $t_{-l'} G_{\text{TE}_{1,0}^z}$  is given by

$$t_{-l'} G_{\text{TE}_{1,0}^z} = \frac{1}{2\pi} \int_{-\infty}^{+\infty} \bar{G}_{\text{TE}_{1,0}^z}(\Delta z, \omega) g(\omega) e^{j\omega(t-l')\Delta t} d\omega \quad (27)$$

with  $g(\omega)$  given by (23) and

$$\bar{G}_{\text{TE}_{1,0}^z}(\Delta z, \omega) = e^{-j\beta_{z,10}\Delta z} \quad (28)$$

where  $\beta_{z,10}$  is calculated by (16) for  $m = 1$  and  $n = 0$ .

#### IV. ABSORBER EVALUATION

To validate the absorber presented herein, we calculate the magnitude of the reflection coefficient in frequency domain for the waveguide structure shown in Fig. 3. The  $xy$ -plane of the waveguide at  $z = 0$  is short circuited and the ABC is utilized to calculate the electric-field components in the  $xy$ -plane at  $z = 2880\Delta z$ . The waveguide cross section is 47.6 mm  $\times$  22 mm and the cell size is given by  $\Delta x = 4.76$  mm,  $\Delta y = 1.1$  mm, and  $\Delta z = 0.4$  mm. We use a mesh of the size  $10 \times 20 \times 2880$  and run the simulation for 25 000 time-steps. All conductors are assumed to be perfect electric conductors (PEC's).

We simulate the wave propagation for frequencies between 3.1–7.4 GHz so that the following three different modes are excited:

- 1)  $\text{TE}_{1,0}^z$ ;
- 2)  $\text{TE}_{2,0}^z$ ;
- 3)  $\text{TE}_{0,1}^z$ .

To accommodate the presence of these three modes, we use a superposition of three Gaussian pulses multiplied with the corresponding mode patterns at  $z = 2840\Delta z$  to provide the correct excitation. For the calculation of the reflection coefficient  $\rho$ , we use the formula

$$\rho = \frac{E_t - E_{\text{ref}}}{E_{\text{ref}}} \quad (29)$$

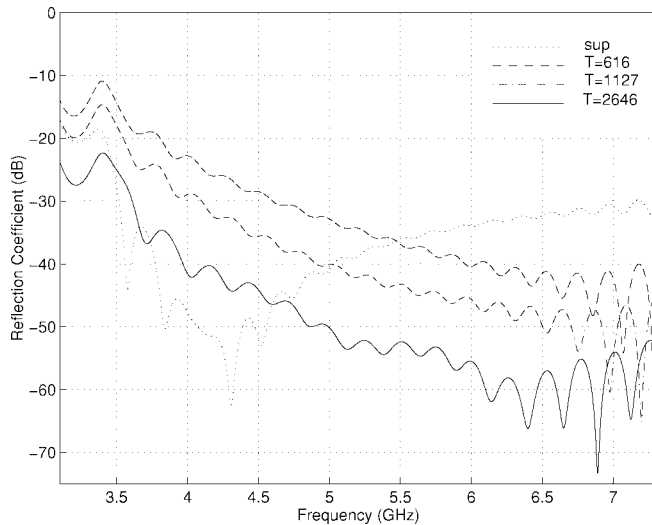


Fig. 4. Reflection coefficient for the  $TE_{1,0}^z$  mode.

where  $E_t$  is the tangential electric field probed at  $z = 2860\Delta z$  and  $E_{\text{ref}}$  is the tangential electric field probed at the same position of a semi-infinitely long waveguide (no effect from reflections from the ABC) with the same cross section. The semi-infinite length of the waveguide is approximated by  $6700\Delta z$  and the tangential electric field is probed again at  $z = 2860\Delta z$ . The evaluated ABC is replaced by a PEC. The length of this reference waveguide is chosen such as no reflections from the PEC plane return to the probe position for the 25 000 steps of simulation. The absorber based on the analytic Green's function is compared to the first-order Mur's ABC coupled with the superabsorption condition. The effective dielectric constant [7] for the superabsorber is chosen to 0.407.

For practical applications, the infinite summation in (25) has to be approximated by a finite number of terms  $T$ . This approximation corresponds to a truncation of the discrete FDTD Green's function according to

$${}_l G_{TE_{m,n}^z} = 0 \quad \text{for } l > T \quad (30)$$

where  $T$  represents the length of the discrete FDTD Green's function with respect to time. We obtain

$$F_{m,n}(n_z, t) = \sum_{\nu=l-T}^l \iota^{-\nu} G_{TE_{m,n}^z} F_{m,n}(n_z - 1, \nu) \quad (31)$$

and (26) can be written as

$$\iota E_{i,j,n_z}^y = \sum_{\nu=l-T}^l \iota^{-\nu} G_{TE_{1,0}^z} E_{1,0}^y(n_z - 1, \nu) \sin(\pi i \Delta x / a). \quad (32)$$

The reflection coefficient is minimized if we truncate the discrete FDTD Green's function at its zeros. In Fig. 4, results for the reflection coefficient for the  $TE_{1,0}^z$  mode are shown for three different values of  $T$ , 616, 1127, and 2646. The graph for the first-order Mur ABC with the superabsorption condition is symbolized with (sup). The larger the length  $T$  of the discrete FDTD Green's function, the more effective

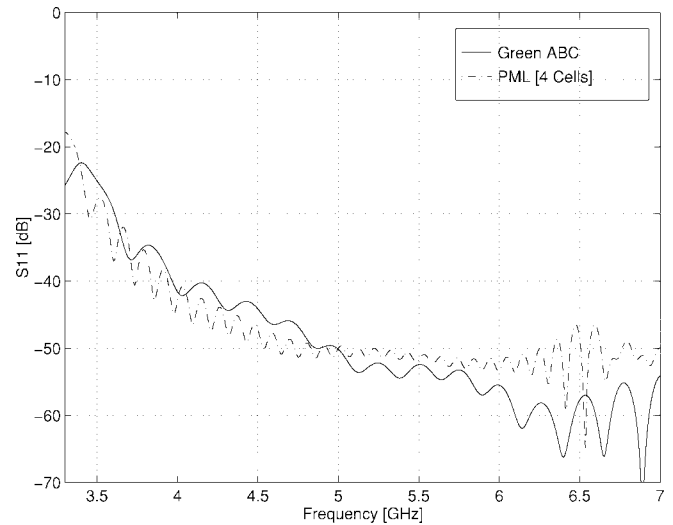


Fig. 5. Comparison of Green's function ABC and PML.

the absorber becomes. For  $T = 2646$ , the amplitude of the reflection coefficient is less than  $-40$  dB for almost the whole frequency range. Thus, the ABC based on the analytic Green's function is effective in a much wider frequency range than the superabsorbing first-order Mur ABC. This is true even when we improve the performance of the superabsorbing first-order Mur ABC by applying it to each waveguide mode separately. Similar results were observed for the reflection coefficient for the  $TE_{2,0}^z$  and  $TE_{0,1}^z$  modes.

The perfectly matched layer (PML) absorber [20] achieves a comparable behavior for a wide frequency range. For example, the length  $T = 2646$  of the discrete  $TE_{1,0}^z$  Green's function offers a reflection coefficient very close to that of a PML layer of four cells with  $R = 10^{-5}$  (see Fig. 5) and  $T = 4161$  has similar performance with a PML layer of eight cells with  $R = 10^{-5}$ . Generally, considering larger values of the length  $T$  is equivalent to increasing the number of the PML cells. Nevertheless, the memory requirements of the absorber proposed in this paper are much lower than the memory requirements for the PML absorber. For each mode, the convolution of (26) requires the storage of the  $T$  terms of the modal Green's function and of the  $T$  previous values of the mode amplitude at the  $z = (n_z - 1)\Delta z$ . Thus, the extra memory requirement of the Green's function absorber is  $2 \times T$  real numbers per mode. A PML layer of  $N$  cells to the  $z$ -direction requires  $M = 6 \times N \times n_x \times n_y$  new variables, where  $n_x \times n_y$  is the grid size for the waveguide cross section. Generally,  $M \gg 2 \times T$ , especially for large grids. Due to the details of the waveguide-probe structure analyzed in Section V, the waveguide cross-section grid has a size of  $477 \times 220$  cells. That means that even a PML layer of four cells to the  $z$ -direction requires the storage of  $M = 2518560$  new variables. Using an absorber based on Green's functions with length  $T = 2646$  for the  $TE_{1,0}^z$ ,  $T = 2238$  for the  $TE_{2,0}^z$ , and  $T = 2412$  for the  $TE_{0,1}^z$ , only 14 592 new variables have to be stored (0.58% of the PML memory requirements). As a result, the Green's-function-based ABC offers a significant economy in memory, while maintaining similar accuracy with the PML absorber.

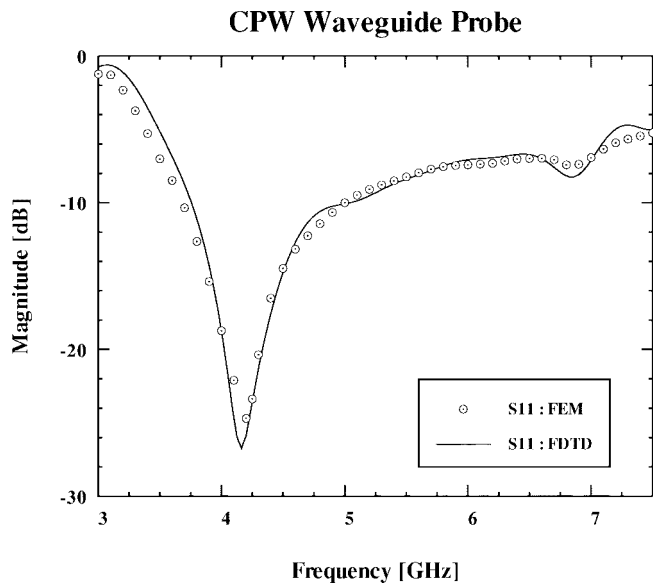


Fig. 6. Validation data for the reflection coefficient.

## V. WAVEGUIDE-PROBE STRUCTURE CHARACTERIZATION

The FDTD technique coupled with the proposed waveguide absorber is used in the RF characterization of the waveguide-probe geometry shown in Fig. 1. The probe in the shape of a rectangular patch is fed by a shielded  $50\text{-}\Omega$  coplanar line and is inserted into the waveguide through a slot. The dielectric substrate carrying the probe is not connected to any waveguide wall. This type of probe can be used as a coupler to a rectangular waveguide or as a diode-mounting structure. The dimensions of the probe, as well as the substrate thickness and the dielectric constant of the substrate, are of critical importance in optimizing coupling to the waveguide.

In our simulations, we try to optimize the thickness of the dielectric substrate carrying a probe which is 3.6-mm wide. The dielectric constant of the substrate is assumed to be  $\epsilon_r = 12$  (GaAs). The width of the dielectric substrate entering the waveguide is 5.8 mm and its thickness is limited to less than 2 mm. The probe is designed to feed a WR-187 rectangular waveguide and, for this reason, excitation is provided on the coplanar feedline by a Gabor function, which covers the frequency range of 3.1–7.4 GHz. For the simulated frequency range, three different modes are excited inside the waveguide— $\text{TE}_{1,0}^z$ ,  $\text{TE}_{2,0}^z$ , and  $\text{TE}_{0,1}^z$ —with the cutoff frequencies 3.15, 6.30, and 6.82 GHz, respectively. The mesh used in the FDTD simulation consists of  $480 \times 477 \times 52$  cells with a time step of  $\Delta t = 0.31425$  ps. The simulation runs for 20000 time steps to achieve converging results. The absorber discussed previously is used to simultaneously absorb all propagating modes of the waveguide for the simulated frequency range.

To characterize the probe performance for different dielectric thicknesses, the magnitude of the reflection coefficient  $|S_{11}|$  for the dominant  $\text{TE}_{1,0}^z$  mode is calculated. For validation purposes, the calculated results are compared to data derived by the FEM assuming a probe width of 3.6 mm and a dielectric thickness of 2.0 mm (see Fig. 6). For the FDTD simulation, the waveguide absorber based on the Green's

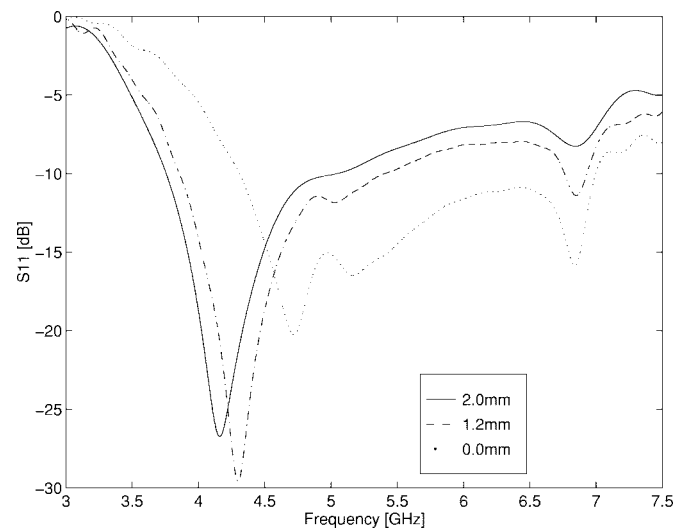


Fig. 7. Reflection coefficient for different dielectric thicknesses.

functions for the three propagating waveguide modes is used at the terminal plane. For the FEM simulation, an artificial absorber depending on frequency and angle of incidence is applied to terminate the waveguide. For the whole operating frequency range (3.1–7.5 GHz), the performance of both absorbers is comparable, and the results show very good agreement.

The dimensions of the shield of the coplanar feedline are chosen to be  $5.8 \text{ mm} \times 3.8 \text{ mm}$ , such as only the coplanar waveguide (CPW) dominant mode can propagate and the field patterns are not disturbed by the sidewalls in the frequency range of the simulation. In this way, the superabsorption condition can be effectively applied at the input plane of the feedline.

The performance of the probe has been evaluated for three different dielectric thicknesses 2.0, 1.2, and 0.0 mm, with the last value corresponding to a microwave probe printed on a dielectric membrane [21]. Results in terms of the reflection coefficient are shown in Fig. 7. As can be observed from Fig. 7, the value of the reflection coefficient reduces over a large frequency range and shows symmetrical behavior around the center design frequency as the dielectric thickness approaches zero. The electric-field ( $E$ ) and magnetic-field ( $H$ ) distributions for zero dielectric thickness are plotted for  $t = 6000$  time steps across the probe structure symmetry plane (see Fig. 8) and across the coplanar feedline plane (see Fig. 9), and represent the transmitted and the reflected energy, respectively.

The reflection coefficient of the Si-membrane printed probe has been calculated for four different patch widths 3.6, 9.8, 11.4, and 13.0 mm, and the results are shown in Fig. 10. From Fig. 10, it can be concluded that the width of 9.8 mm offers the most symmetrical behavior for the frequency of operation. The reflection coefficient for widths larger than 9.8 mm is much smaller than that of 3.6 mm for most of the simulated frequencies, except a small region round 4.6 GHz. Nevertheless, the widths of 11.4 and 13.0 mm offer no significant improvement over the width of 9.8 mm.

Another geometry parameter of the Si-membrane printed probe that has been investigated is the distance of the probe

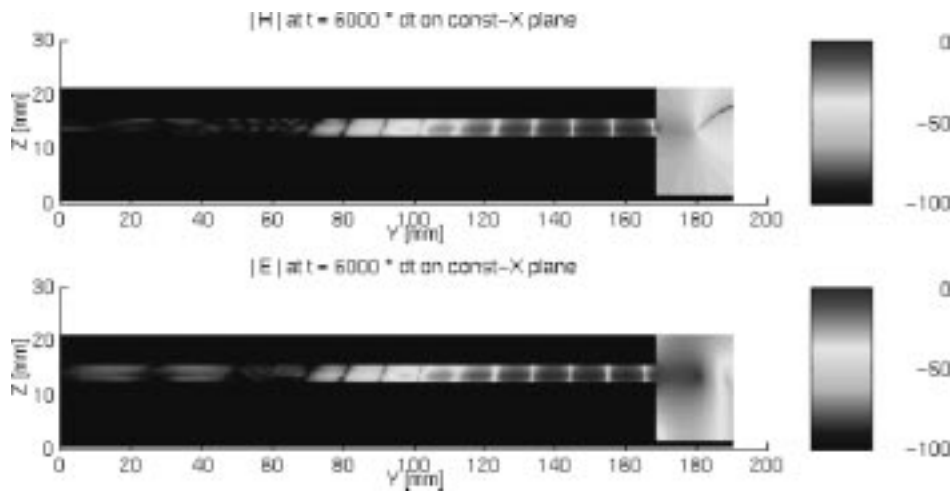


Fig. 8.  $E$ - and  $H$ -field distributions across the probe-structure symmetry plane.

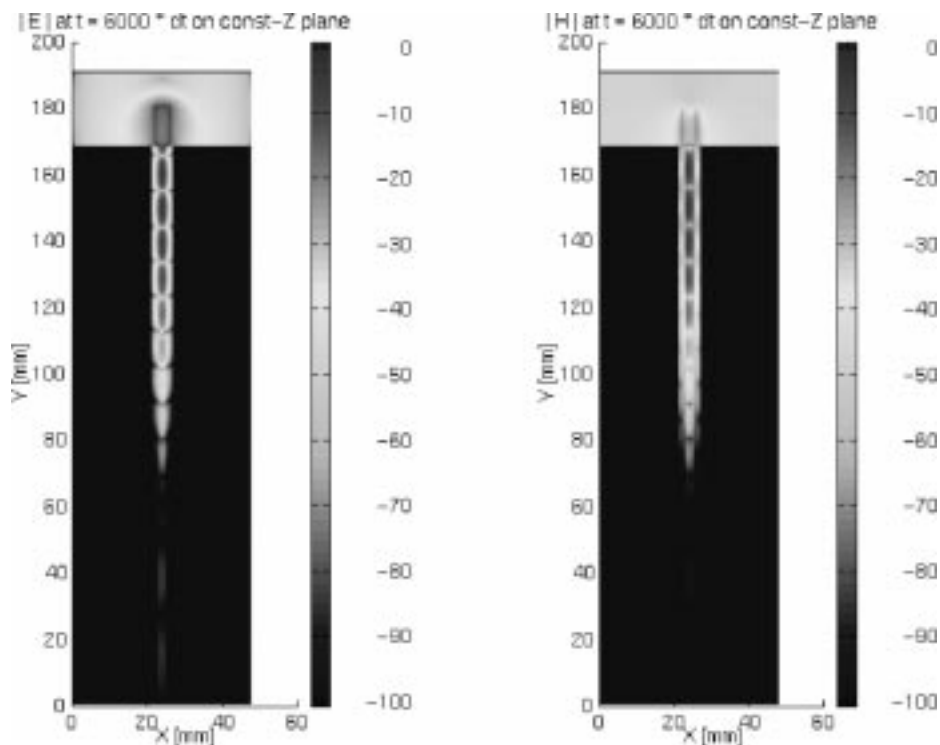


Fig. 9.  $E$ - and  $H$ -field distributions across the coplanar feedline plane.

patch from the short circuit of the waveguide. Lengths of 8.8, 10.4, 12.0, and 13.6 mm have been used, and the results are plotted in Fig. 11. It can be noticed that the value of 12.0 mm offers the best performance in terms of the value and bandwidth of the reflection coefficient.

The FDTD results derived by using the absorber presented in Section III have been validated by comparison to experimental data. The probe has dimensions  $13.2 \text{ mm} \times 4.3 \text{ mm}$  on a dielectric substrate with thickness 2.1 mm, width 28.7 mm, and  $\epsilon_r = 13$ . The probe has been inserted in a WR229 waveguide and is located at a distance of 14.7 mm from the top-surface short circuit. For the FDTD absorber,  $T = 2871$  time steps have been used. The performance of the probe has been evaluated for the frequency range of 3.3–4.6 GHz, and the results are shown in Figs. 12 and 13. The agreement between

the FDTD and experimental results is good, especially in the frequency range of the optimum performance of the probe. The abrupt variation in  $S_{21}$  observed for the higher frequencies in the experiment is perhaps due to calibration or other reasons related to the experimental setup.

## VI. CONCLUSION

The FDTD method has been used to analyze a waveguide-probe structure. For the analysis, a waveguide absorber based on analytic Green's functions has been developed. This absorber is characterized by a better performance in accuracy and computational efficiency than the superabsorbing first-order Mur ABC, and by a better performance in memory requirements than the PML absorber. The scattering parameters of the probe structure have been calculated, and the results have

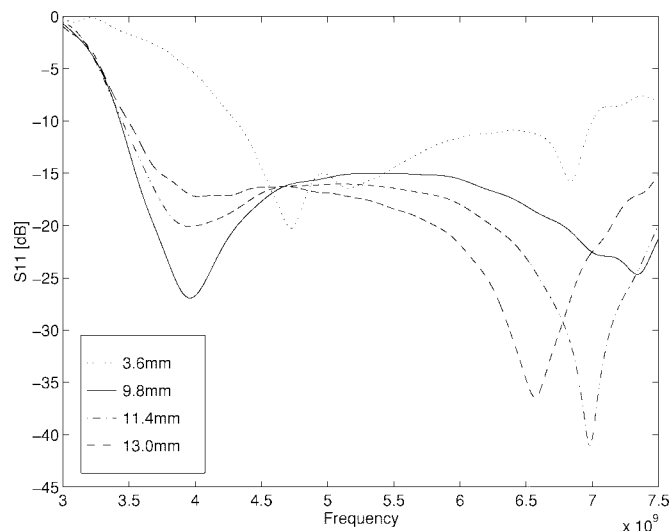


Fig. 10. Reflection coefficient for different patch widths.

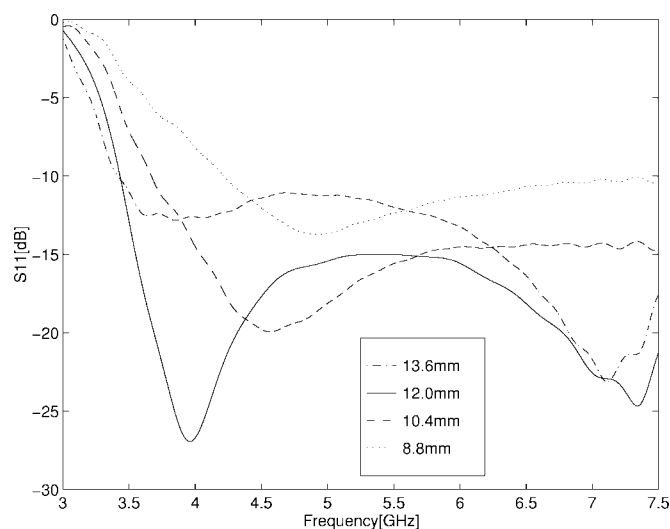
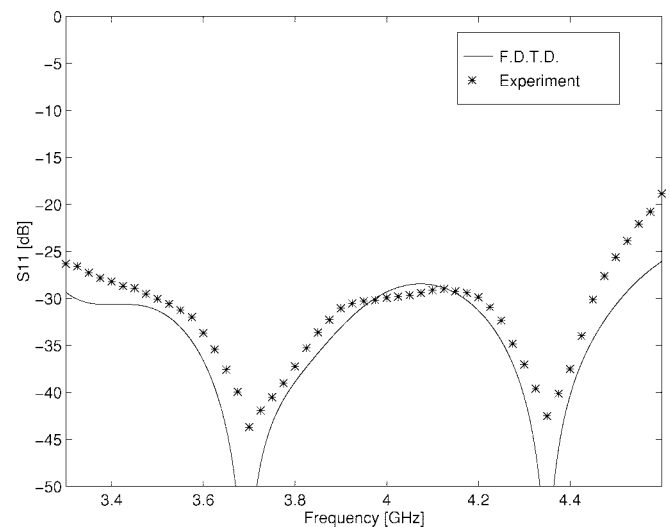
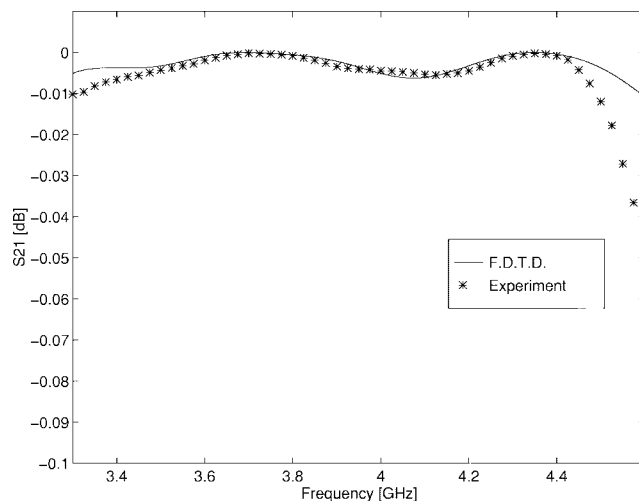


Fig. 11. Reflection coefficient for different distances from the top surface short circuit.

Fig. 12. Experimental validation for  $S_{11}$ .Fig. 13. Experimental validation for  $S_{21}$ .

been verified by comparison with the FEM and experimental data. The influence of critical geometrical parameters on the probe performance has been investigated and optimized.

#### ACKNOWLEDGMENT

The authors acknowledge the continued support of the NASA Center for Space Terahertz Technology, Radiation Laboratory, University of Michigan at Ann Arbor.

#### REFERENCES

- [1] J. M. Rollins and J. M. Jarem, "The input impedance of a hollow-probed, semi-infinite rectangular waveguide," *IEEE Trans. Microwave Theory Tech.*, vol. 37, pp. 1144–1146, July 1989.
- [2] A. G. Williamson, "Coaxially fed hollow probe in a rectangular waveguide," *Proc. Inst. Elect. Eng.*, vol. 132, pt. H, pp. 273–285, 1985.
- [3] W. W. S. Lee and E. K. N. Yung, "The input impedance of a coaxial line fed probe in a cylindrical waveguide," *IEEE Trans. Microwave Theory Tech.*, vol. 42, pp. 1468–1473, Aug. 1994.
- [4] E. Tentzeris, N. Dib, L. Katehi, J. Oswald, and P. Siegel, "Time-domain characterization of diode-mounting structures," in *NASA Terahertz Symp. Dig.*, Ann Arbor, MI, Mar. 1994.
- [5] K. S. Yee, "Numerical solution of initial boundary value problems involving Maxwell's equations in isotropic media," *IEEE Trans. Antennas Propagat.*, vol. AP-14, pp. 302–307, May 1966.
- [6] G. Mur, "Absorbing boundary conditions for the finite-difference approximation of the time-domain electromagnetic-field equations," *IEEE Trans. Electromag. Compat.*, vol. EMC-23, pp. 377–382, Nov. 1981.
- [7] K. K. Mei and J. Fang, "Superabsorption—A method to improve absorbing boundary conditions," *IEEE Trans. Antennas Propagat.*, vol. 40, pp. 1001–1010, Sept. 1992.
- [8] P. B. Johns and K. Aktharzad, "The use of time domain diakoptics in time discrete models of fields," *Int. J. Numer. Meth. Eng.*, vol. 17, pp. 1–14, 1981.
- [9] W. J. R. Hoefler, "The discrete time domain Green's function or Johns' matrix—A new powerful concept in transmission line modeling (TLM)," *Int. J. Num. Modeling*, vol. 2, pp. 215–225, 1989.
- [10] T. W. Huang, B. Housmand, and T. Itoh, "The implementation of time-domain diakoptics in the FDTD method," *IEEE Trans. Microwave Theory Tech.*, vol. 42, pp. 2149–2155, Nov. 1994.
- [11] C. Eswarappa and W. J. R. Hoefler, "Diakoptics and wideband dispersive absorbing boundaries in the 3-D TLM method with symmetrical condensed node," *IECE Trans.*, vol. E74, no. 5, pp. 1242–1250, May 1991.
- [12] M. Righi and W. J. R. Hoefler, "Efficient 3D-SCN-TLM diakoptics for waveguide components," *IEEE Trans. Microwave Theory Tech.*, vol. 42, pp. 2381–2385, Dec. 1994.
- [13] M. Righi, W. J. R. Hoefler, M. Mongiardo, and R. Sorrentino, "Efficient TLM diakoptics for separable structures," *IEEE Trans. Microwave Theory Tech.*, vol. 43, pp. 854–859, Apr. 1995.

- [14] M. Werthen, M. Rittweger, and I. Wolff, "FDTD-simulation of waveguide junctions using a new boundary condition for rectangular waveguides," in *Proc. 24th European Microwave Conf.*, Cannes, France, 1994, pp. 1715-1719.
- [15] F. Moglie, T. Rozzi, P. Marcozzi, and A. Schiavoni, "A new termination condition for the application of FDTD techniques to discontinuity problems in close homogeneous waveguide," *IEEE Microwave Guided Wave Lett.*, vol. 2, pp. 475-477, Dec. 1992.
- [16] M. Krumpolz, B. Bader, and P. Russer, "On the theory of discrete TLM Green's functions in three-dimensional TLM," *IEEE Trans. Microwave Theory Tech.*, vol. 43, pp. 1472-1483, July 1995.
- [17] M. Werthen, M. Rittweger, and I. Wolff, "Multi-mode simulation of homogeneous waveguide components using a combination of the FDTD and  $FD^2$  method," in *Proc. 25th European Microwave Conf.*, Bologna, Italy, 1995, pp. 234-237.
- [18] M. Schwarz, *Information, Transmission, Modulation and Noise* (McGraw-Hill Int. Editions Series), 7th ed. New York: McGraw-Hill, 1987, pp. 72-76.
- [19] M. Krumpolz, C. Huber, and P. Russer, "A field theoretical comparison of FDTD and TLM," *IEEE Trans. Microwave Theory Tech.*, vol. 43, pp. 1935-1950, Aug. 1995.
- [20] J.-P. Berenger, "A perfectly matched layer for the absorption of electromagnetic waves," *J. Comput. Phys.*, vol. 114, pp. 185-200, 1994.
- [21] C.-Y. Chi and G. M. Rebeiz, "Planar microwave and millimeter-wave lumped elements and couple-line filters using micro-machining techniques," *IEEE Trans. Microwave Theory Tech.*, vol. 44, pp. 730-738, Apr. 1995.



**Emmanouil Tentzeris** (M'91), was born in Piraeus, Greece, in 1970. He received the Electrical Engineering and Computer Science Diploma Degree (*Suma cum laude*) from the National Technical University of Athens (NTUA), Athens, Greece, in 1992, and the M.Sc. and Ph.D. Degrees from the University of Michigan at Ann Arbor, in 1993 and 1998 respectively.

From 1992 to 1998, he was a Graduate Research Assistant with the Radiation Laboratory, University of Michigan. He is currently an Assistant Professor

with the School of Electrical and Computer Engineering, Georgia Institute of Technology, Atlanta. He has authored or co-authored over 25 papers in refereed journals and conference proceedings. His research interests include the development of novel numerical techniques and the application of the principles of multiresolution analysis in the simulation of microwave circuits used in wireless or satellite communication systems.

Dr. Tentzeris is a member of the Technical Chamber of Greece. He received the Best Paper Award from the International Microelectronics and Packaging Society (IMAPS) in 1997.

**Michael Krumpolz** (M'94) was born in Bonn, Germany, in 1966. He received the Dipl.-Ing. and Dr.-Ing. degrees in electrical engineering from the Technische Universität Aachen, Aachen, Germany, in 1991 and 1994.

From 1991 to 1992, he was with the Lehrstuhl für Hochfrequenztechnik, Technische Universität München, Munich, Germany. In 1992, he joined the Ferdinand-Braun-Institut für Hochfrequenztechnik, Berlin, Germany. From 1994 to 1995, he was with the Radiation Laboratory, University of Michigan in Ann Arbor. Since September 1995, he has been with the Daimler-Benz Corporation, Stuttgart, Germany.

**Nihad Dib** (S'89-M'92) received the B.Sc. and M.Sc. degrees in electrical engineering from Kuwait University, Kuwait, in 1985 and 1987, respectively, and the Ph. D. degree in electrical engineering from the University of Michigan at Ann Arbor, in 1992.

From 1993 to 1995, he was an Assistant Research Scientist in the Radiation Laboratory, University of Michigan. In September 1995, he joined the Electrical Engineering Department, Jordan University of Science and Technology, Irbid, Jordan, as an Assistant Professor. His research interests include the numerical analysis and modeling of planar microwave circuits.



**Jong-Gwan Yook** was born in Korea, in 1964. He received the B.S. and M.S. degrees in electronic engineering from Yonsei University, Seoul, Korea, in 1987 and 1989, respectively, and Ph.D. degree from the University of Michigan at Ann Arbor, in 1996.

He is currently with the Radiation Laboratory, Department of Electrical Engineering and Computer Science, University of Michigan at Ann Arbor, as a Research Fellow. His main research interests are in the area of theoretical/numerical electromagnetic modeling and characterization of microwave/millimeter-wave circuits and components, very large scale integration (VLSI) and monolithic-microwave integrated-circuit (MMIC) interconnects using frequency and time-domain full-wave methods, and development of numerical techniques for analysis and design of high-speed high-frequency circuits with emphasis on parallel/super computing.



**Linda P. B. Katehi** (S'81-M'84-SM'89-F'95) received the B.S.E.E. degree from the National Technical University of Athens, Athens, Greece, in 1977, and the M.S.E.E. and Ph.D. degrees from the University of California at Los Angeles, in 1981 and 1984, respectively.

In September 1984, she joined the faculty of the Electrical Engineering and Computer Science Department, University of Michigan at Ann Arbor. Since then, she has been interested in the development and characterization (theoretical and experimental) of microwave, millimeter printed circuits, the computer-aided design of VLSI interconnects, the development and characterization of micro-machined circuits for millimeter-wave and submillimeter-wave applications, and the development of low-loss lines for terahertz-frequency applications. She has also been theoretically and experimentally studying various types of uniplanar radiating structures for hybrid-monolithic and monolithic oscillator and mixer designs.

Dr. Katehi is a member of IEEE Antennas and Propagation and IEEE Microwave Theory and Techniques Societies, Sigma Xi, Hybrid Microelectronics, URSI Commission D, and a member of IEEE AP-S AdCom (1992-1995). She is an associate editor for the IEEE TRANSACTIONS ON MICROWAVE THEORY AND TECHNIQUES. She was awarded the IEEE AP-S R. W. P. King Best Paper Award for a Young Engineer in 1984, A. Schelkunoff Best Paper Award in 1985, the NSF Presidential Young Investigator Award and URSI Young Scientist Fellowship in 1987, the Humboldt Research Award and The University of Michigan Faculty Recognition Award in 1994, the IEEE MTT-S Microwave Prize in 1996, and the International Microelectronics and Packaging Society (IMAPS) Best Paper Award in 1997.